JEM Journal of Experimental Medicine

ARTICLE

Monocyte-derived macrophages promote breast cancer bone metastasis outgrowth

Ruo-Yu Ma[1], Hui Zhang[2], Xue-Feng Li[1], Cheng-Bin Zhang[1], Cigdem Selli[1], Giulia Tagliavini[3], Alyson D. Lam[1], Sandrine Prost[3], Andrew H. Sims[4], Hai-Yan Hu[5], Tianlei Ying[6], Zhan Wang[7], Zhaoming Ye[7], Jeffrey W. Pollard[1,2], and Bin-Zhi Qian[1,4,8]

Bone metastasis is the major cause of death in breast cancer. The lack of effective treatment suggests that disease mechanisms are still largely unknown. As a key component of the tumor microenvironment, macrophages promote tumor progression and metastasis. In this study, we found that macrophages are abundant in human and mouse breast cancer bone metastases. Macrophage ablation significantly inhibited bone metastasis growth. Lineage tracking experiments indicated that these macrophages largely derive from Ly6C$^+$CCR2$^+$ inflammatory monocytes. Ablation of the chemokine receptor, CCR2, significantly inhibited bone metastasis outgrowth and prolonged survival. Immunophenotyping identified that bone metastasis–associated macrophages express high levels of CD204 and IL4R. Furthermore, monocyte/macrophage-restricted IL4R ablation significantly inhibited bone metastasis growth, and IL4R null mutant monocytes failed to promote bone metastasis outgrowth. Together, this study identified a subset of monocyte-derived macrophages that promote breast cancer bone metastasis in an IL4R-dependent manner. This suggests that IL4R and macrophage inhibition can have potential therapeutic benefit against breast cancer bone disease.

Introduction

Macrophages potently promote breast cancer progression and act at all steps of the metastasis cascade (Kitamura et al., 2015b; Qian and Pollard, 2010). However, these cells are heterogeneous, and their phenotype and function are tightly regulated by the local tissue environment (Gordon and Plüddemann, 2019). It has become evident that most tissue-resident macrophages originate from embryonic precursor cells that can persist through life. In some cases, they are replaced or complemented by bone marrow–derived precursor cells, monocytes. In contrast, adult macrophages in pathophysiological situations are largely derived from monocytes (Wynn et al., 2013). Several studies, including our own, indicate that monocyte-derived macrophages are critical for tumor growth and metastasis (Afik et al., 2016; Franklin et al., 2014; Lin et al., 2001; Qian et al., 2011). However, in some cases, tissue-resident macrophages can also have an important function in tumor promotion (Zhu et al., 2017). Therefore, a better understanding of the origin and function of macrophage subsets in different cancer types and secondary organs is critical for developing precise treatment to maximize clinical benefit.

Bone metastasis is the most prevalent form of metastasis in breast cancer and accounts for >70% of cases (Coleman, 2001). It causes bone pain, bone loss, fracture, and other skeletal related events that dramatically impair the patient's quality of life, and it is lethal (Coleman, 2006; Weilbaecher et al., 2011). Although current therapeutic modalities such as radiotherapy, chemotherapy, and antiosteolytic agents can reduce morbidity associated with bone metastasis, these treatments often provide only a minimum survival benefit to patients (Weilbaecher et al., 2011). This indicates that a better understanding of the mechanisms that lead to bone metastasis outgrowth will be critical for the development of effective treatment. Recent studies strongly argue that intricate interaction between tumor cells and the supportive stroma play important roles in the development of

[1]Medical Research Council Centre for Reproductive Health, College of Medicine and Veterinary Medicine, Queen's Medical Research Institute, The University of Edinburgh, Edinburgh, UK; [2]Department of Developmental and Molecular Biology, Albert Einstein College of Medicine, New York, NY; [3]Medical Research Council Centre for Inflammation Research, College of Medicine and Veterinary Medicine, Queen's Medical Research Institute, The University of Edinburgh, Edinburgh, UK; [4]Edinburgh Cancer Research UK Centre, Institute of Genetics & Molecular Medicine, University of Edinburgh, Edinburgh, UK; [5]Shanghai Jiao Tong University Affiliated Sixth People`s Hospital, Shanghai, China; [6]Ministry of Education/National Health Commission/Chinese Academy of Medical Sciences Key Laboratory of Medical Molecular Virology, School of Basic Medical Sciences, Shanghai Medical College, Fudan University, Shanghai, China; [7]Department of Orthopaedics, Centre for Orthopaedic Research, Orthopaedics Research Institute of Zhejiang University, The Second Affiliated Hospital, Zhejiang University School of Medicine, Zhejiang, China; [8]Guangdong Provincial Education Department Key Laboratory of Nano-immunoregulation Tumor Microenvironment, The Second Affiliated Hospital, Guangzhou Medical University, Guangzhou, Guangdong, China.

Correspondence to Bin-Zhi Qian: binzhi.qian@ed.ac.uk; Jeffery W. Pollard: jeff.pollard@ed.ac.uk.

this deadly disease (Liu et al., 2019; Price et al., 2016; Sethi et al., 2011; Wang et al., 2015; Wu et al., 2017). For example, the osteogenic niche composed of bone-building osteoblasts has recently been shown to be critical for the survival and colonization of disseminated tumor cells in the bone (Shiozawa et al., 2011; Wang et al., 2015). However, the specific role of macrophage subsets in breast cancer bone metastasis is largely unknown.

In the current study, our data indicate that macrophages are critical for bone metastasis outgrowth in vivo. Combining genetic ablation models of CC chemokine receptor 2 (*Ccr2*$^{-/-}$), IL-4 receptor (*Il4r*$^{-/-}$), and a monocyte add-back approach, we have identified that a population of monocyte-derived macrophages, rather than bone-resident macrophages, promote breast cancer bone metastasis outgrowth in an IL4R-dependent manner.

Results

Macrophage targeting inhibits bone metastasis outgrowth in breast cancer

To determine the infiltration of macrophages in patient bone metastasis samples, we stained a small cohort of patient samples (for patient information, see Table S1) with CD68, a commonly used macrophage marker. All patient samples showed significant amounts of macrophage infiltration (472.8 ± 189.7 macrophages/mm^2 tumor area; Fig. 1 A). Similar levels of macrophage infiltration detected by Iba1 staining are observed in a widely used in vivo model of bone metastasis using 1833 cells (a subline of MDA-MB-231 human triple-negative breast cancer cells; Kang et al., 2003) in nude mice. This infiltration is also found in bone metastasis derived from MetBo2 cells, a newly developed bone metastasis cell line derived from polyoma middle T oncogene–induced mouse mammary tumor on a syngeneic Friend Virus B NIH Jackson (FVB) background (Fig. 1 B). These results confirm that these two models have a similar level of macrophage infiltration as seen in patient bone metastasis.

Bone metastasis outgrowth leads to macrometastatic lesions that significantly impair patient survival and quality of life. To determine the role of macrophages in bone metastasis outgrowth, we adopted a widely used in vivo macrophage-ablation method of treating mice with liposome-encapsulated clodronate (L-Clod; Van Rooijen and Sanders, 1994; Qian et al., 2009) after tumor detection in the MetBo2 and 1833 models (Fig. 1, C and D). As expected, L-Clod treatment significantly depleted macrophages in bone metastasis without affecting other immune cell populations compared with the treatment with control liposome-PBS (L-PBS; Fig. S1 A). Such macrophage ablation with L-Clod that was performed after detection of established MetBo2 cell bone lesions significantly inhibited metastasis outgrowth in syngeneic FVB mice (Fig. 1 D). Colony-stimulating factor 1 receptor (CSF1R) is a critical lineage receptor for macrophage differentiation and function in vivo (Stanley et al., 1997). Using a specific small-molecule CSF1R inhibitor, BLZ945, we observed a significant inhibition of bone metastasis growth of MetBo2 cells in syngeneic FVB mice compared with vehicle treatment (Fig. 1 E). Similarly, BLZ945 significantly inhibited bone metastasis growth of 1833 cells in nude mice (Fig. 1 F). Consistent with their mode of action, BLZ945 and L-Clod significantly reduced macrophage abundance in bone lesions without affecting other major immune cell populations (Fig. S1 B).

Osteoclasts, specialized cells of the macrophage lineage, have been shown to engage in paracrine signaling with cancer cells that promote breast cancer bone disease (Maurizi and Rucci, 2018). These cells were also depleted by L-Clod treatment (Fig. S2 A). These data revealed that although L-Clod was originally designed to target phagocytic macrophages that actively uptake liposomes (Van Rooijen and Sanders, 1994), it also affects osteoclasts. Therefore, it is possible that part of the metastasis-inhibiting effect observed in our experiments is through inhibition of osteoclasts. Soluble/free clodronate (not encapsulated in liposome) is known to target osteoclasts because of its high affinity to bone. This treatment was effective (Fig. S2 B), as expected, and did not affect infiltration of bone metastasis–associated macrophages (BoMAMs) in our models (Fig. S1 C). Although osteoclast inhibition with free clodronate alone can inhibit bone metastatic growth of MetBo2 cells, the inhibition was 2.4-fold more effective with L-Clod, which depleted both osteoclasts and BoMAMs (Fig. S2 D). Together, these data support the conclusion that BoMAMs can directly promote metastatic outgrowth independently of osteoclasts and that macrophage ablation can effectively inhibit bone metastasis outgrowth in vivo.

CCL2-recruited inflammatory monocytes (IMs) promote bone metastasis growth

Macrophages in most tissues can be derived from both bone marrow monocyte precursor cells and tissue-resident macrophages originated from yolk sac precursor cells (Cassetta and Pollard, 2018; Schulz et al., 2012). Tissue-resident macrophages with a profibrotic phenotype have been shown to promote tumor progression in pancreatic cancer models (Zhu et al., 2017). Bone marrow–resident macrophages express CD169 as a cell surface marker (Batoon et al., 2019; Hashimoto et al., 2013). In our model, CD169$^+$ macrophages were mainly associated with tumor-adjacent stroma (Fig. S3 A). These CD169$^+$ macrophages could be efficiently depleted in transgenic mice expressing diphtheria toxin (DT) receptor under the control of CD169 promoter (CD169-DTR) upon DT treatment (Fig. S2, B and C), which led to a significant reduction of total macrophage numbers (Fig. S3 B) compared with control treatment with a mutant toxin (Glu52-mutated DT [Glu-DT]) which, because of a point mutation, does not bind to the DT receptor. This ablation did not affect bone metastasis growth (Fig. S3 C). Immunofluorescent staining showed a significant ablation of CD169$^+$ macrophages without affecting the majority of tumor-infiltrating macrophages labeled by the lineage marker, Iba1 (Fig. S3 D). This indicates that bone-resident macrophages do not play a major role in our model and strongly suggests that tumor-promoting BoMAMs were derived mainly from recruited monocytes.

Monocytes are heterogeneous, and the two most well-characterized populations in mice are Ly6C-expressing IMs (classical monocytes) and patrolling monocytes (PMs; nonclassic or resident monocytes) lacking Ly6C (Auffray et al., 2009; Geissmann et al., 2010). To understand the origin of BoMAMs, we measured monocyte recruitment after adoptive transfer of

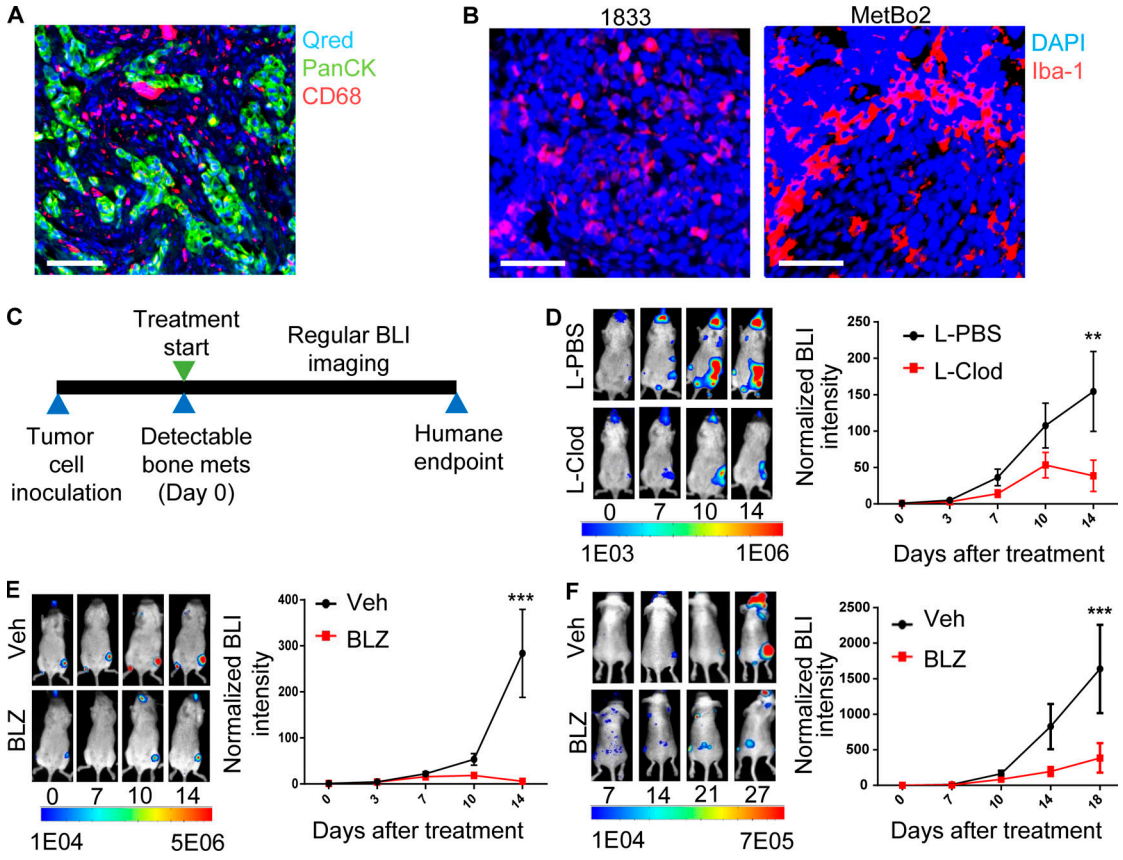

Figure 1. **MAMs depletion inhibits bone metastasis outgrowth. (A)** Representative immunofluorescent staining of CD68$^+$ macrophages (red) infiltrated in PanCK$^+$ tumor area (green) of human breast cancer bone metastasis sample. Nuclei were stained with Qred. Scale bar = 20 µm. *n* = 9 from two independent experiments. **(B)** Representative immunofluorescent staining of Iba1$^+$ macrophages (red) in bone metastasis of 1833 human breast cancer cells (left) and MetBo2 murine breast cancer cells (right). Bar = 20 µm. Nuclei were stained with DAPI (blue). Experiments performed two times independently. **(C)** Diagram of macrophage depletion in established bone metastasis detected by bioluminescent (BLI) imaging with the L-clodronate treatment indicated until the humane end point. **(D)** Representative images and quantification of bioluminescent signal of MetBo2 bone metastasis treated with L-Clod or corresponding vehicle (L-PBS). Signals were quantified by PhotonIMAGER and normalized to day 0. Bar represents SEM; *n* = 6–8 mice for each group. **, P < 0.01 with Student's *t* test. Experiments performed three times independently. **(E)** Representative figures and quantification of bioluminescent signal of MetBo2 bone metastasis treated with BLZ945 (BLZ) or corresponding vehicle (Veh). Signals were quantified by PhotonIMAGER and normalized to day 0. Bar represents SEM; *n* = 6–8 mice for each group. ***, P < 0.001 with Student's *t* test. Experiments performed three times independently. **(F)** Representative figures and quantification of bioluminescent signal of 1833 bone metastasis treated with BLZ945 (BLZ) or corresponding vehicle (Veh). Signals were quantified by PhotonIMAGER and normalized to day 0. Bar represents SEM; *n* = 6–8 mice for each group. ***, P < 0.001 with Student's *t* test. Experiments performed two times independently.

each subset. Mouse monocytes were identified by their expression of CD11b and CD115 and were FACS sorted into IMs and PMs based on Ly6C expression. As previously reported, both populations have similar levels of GFP expression in *Csf1r*–GFP transgenic mice (Qian et al., 2011). We adoptively transferred 10^5 cells of each population into syngeneic FVB mice bearing bone metastasis of MetBo2 cells or healthy mice as controls (Fig. 2 A). 18 h after adoptive transfer, we determined the number of GFP-positive monocytes in the bone to measure their relative recruitment. Our previous studies have shown that at this time point, similar numbers of donor cells are present in the blood, showing equivalent availability (Qian et al., 2011). In healthy bone morrow, these two populations were recruited to a comparable level. However, in bone metastases, IMs were preferentially recruited, with approximately twofold enrichment (Fig. 2 B).

CCL2 and CC chemokine receptor 2 (CCR2) signaling is the major chemoattractant that mediates the recruitment of Ly6C$^+$ IMs (Getts et al., 2008; Palframan et al., 2001). Consistent with a previous report (Shi et al., 2011), circulating IMs were significantly reduced in *Ccr2*$^{-/-}$ mice compared with *Ccr2*$^{+/-}$ or WT littermates (Fig. S4 A), but this reduction was not observed in the bone marrow (Fig. S4 B). The bone colonization efficiency of MetBo2 cells was significantly inhibited in *Ccr2*$^{-/-}$ mice, leading to reduced metastatic growth and prolonged survival of mice compared with WT controls (Fig. 2, C and D). Consistent with these data, the bone colonization efficiency of 1833 cells was also significantly inhibited in mice with CCR2 knockout compared with WT controls (Fig. 2, E and F). Furthermore, CCL2 blockade using neutralizing antibody 48 h after tumor cell inoculation significantly inhibited 1833 bone metastasis growth (Fig. 2 G). Because our previous studies indicate that tumor cell metastatic extravasation and seeding mostly occur within 36 h after reaching the distal organ, these data strongly suggest that recruitment of IMs is critical for tumor metastatic outgrowth after

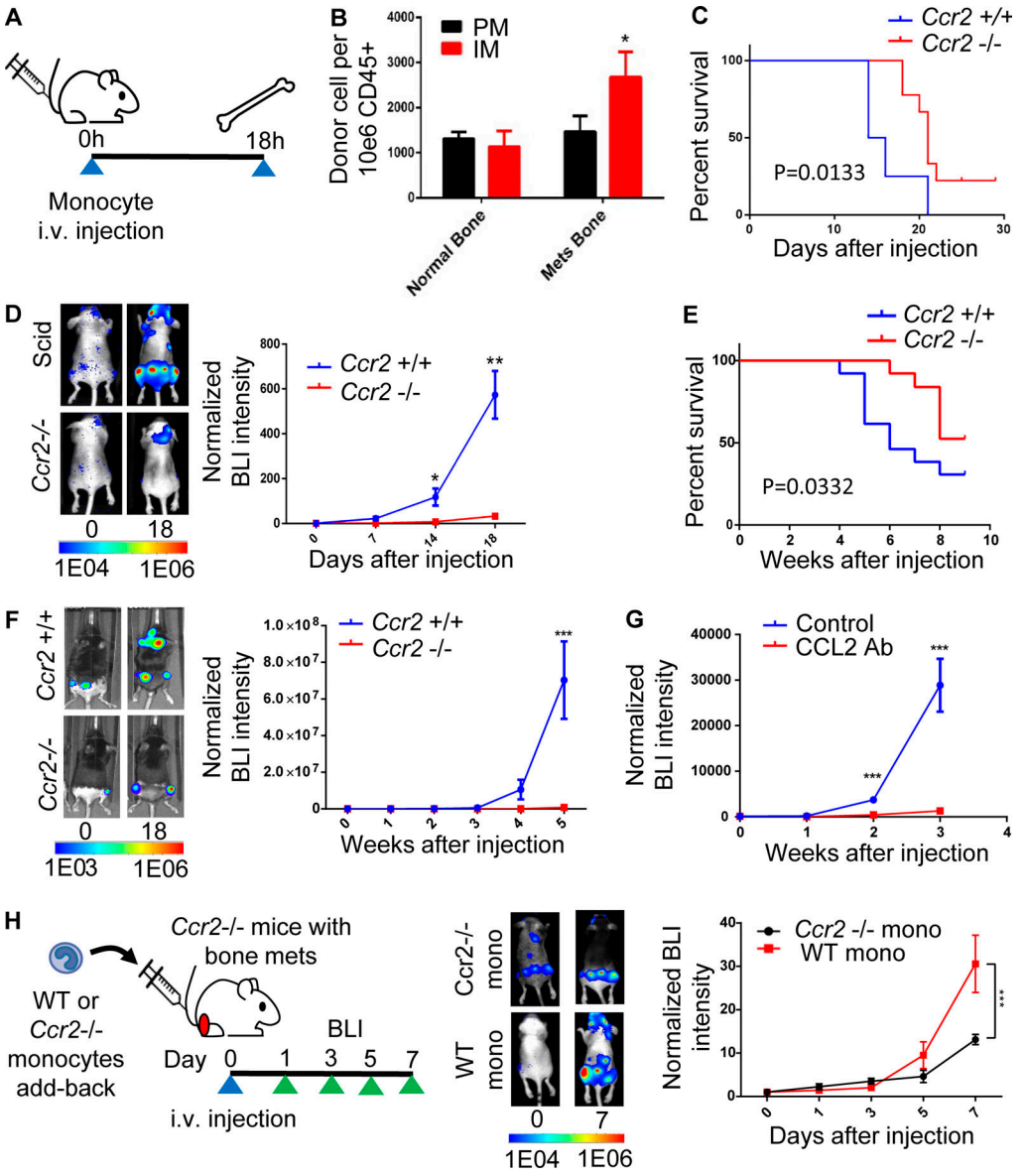

Figure 2. **CCL2-recruited IMs promote bone metastasis growth. (A)** Diagram of adoptive transfer of monocytes in healthy mice and mice with bone metastasis. **(B)** Relative number of recruited IMs and PMs in bone of recipient mice bearing bone metastasis or healthy controls. *n* = 6; *, P < 0.05 with Student's *t* test. Experiments performed two times independently. **(C)** Survival curve (defined as time taken to reach the humane end point) of mice with MetBo2 bone metastasis. WT, *n* = 4; knockout, *n* = 9; P = 0.0133. **(D)** Representative images and quantification of bioluminescent (BLI) signal for MetBo2 bone metastasis in *Ccr2*$^{-/-}$ mice and WT mice. Signals were quantified by PhotonIMAGER and normalized to day 0. *Ccr2*$^{-/-}$ group, *n* = 8 mice; WT group, *n* = 7 mice. Bar represents SEM. **, P < 0.01 with Student's *t* test. Experiments performed four times independently. **(E)** Survival curve of mice with bone metastasis. Death is defined as time the mice take to reach the humane end point. P = 0.0332. **(F)** Representative images and quantification of bioluminescent signal for 1833 human bone metastasis model in *Ccr2*$^{-/-}$ mice and WT mice. Signals were measured by IVIS and normalized to day 0. *Ccr2*$^{-/-}$ group, *n* = 8 mice; control group, *n* = 7 mice. Bar represents SEM. ***, P < 0.001 with Student's *t* test. **(G)** Quantification of bioluminescent signal for 1833 human bone metastasis model treated with anti-CCL2 inhibitory antibody (Ab) or corresponding isotype control (IgG). Signals were measured by IVIS and normalized to day 0. CCL2 antibody–treated group, *n* = 8 mice; control group, *n* = 7 mice. Bar represents SEM. ***, P < 0.001 with Student's *t* test. **(H)** Diagram and quantification of bioluminescent signal of monocyte add-back. Recipient mice are *Ccr2*-deficient mice with 1833 bone metastasis. Monocytes from WT mice and *Ccr2*-deficient mice were injected i.v. after tumor signal was detected. Bioluminescent signals on the legs were quantified by PhotonIMAGER and normalized to day 0. Each group contain data from four legs. Bar represents SEM. ***, P < 0.001 with Student's *t* test. *n* = 4–5. Experiments performed three times independently.

seeding. To further test this, we established bone metastasis of MetBo2 cells in *Ccr2*$^{-/-}$ mice, which have deficiency in circulating monocytes and delayed tumor growth. Upon bone metastasis detection, add-back of WT IMs via adoptive transfer significantly promoted tumor outgrowth compared with *Ccr2*$^{-/-}$ monocytes (Fig. 2 H). Together, these data indicate that CCL2/CCR2-dependent recruitment of IMs is critical for breast cancer bone metastasis outgrowth.

BoMAMs bear distinct cell surface markers

To further characterize the BoMAMs, we performed gene expression profiling of macrophages isolated from bone metastasis

and identified 409 up-regulated genes and 527 down-regulated genes compared with macrophages from healthy bone, with a threshold of 1.5-fold change and $P < 0.05$ (Fig. 3 A). For major macrophage polarization marker genes, macrophages associated with bone metastasis express higher levels of some alternative activation markers (e.g., *Il4ra* and *Il10*), but also some of the classic activation markers (e.g., *Tnf* and *Il1b*; Fig. 3 B) compared with their counterparts from healthy bone. Further analysis indicated up-regulation of genes related to several tumor-promoting functions, such as angiogenesis, tumor growth, cancer stem cells, immune suppression, etc., in BoMAMs compared with normal counterparts (Fig. 3 C). These results are consistent with previous reported tumor promotion functions of macrophages in other contexts (Cassetta et al., 2019; Ojalvo et al., 2009; Yang et al., 2018). Immunophenotyping of macrophages (defined by $CD45^+CD11b^+F4/80^+Ly6C^-Ly6G^-SSC^{lo}$; Chow et al., 2011) isolated from bone metastasis of MetBo2 cells and adjacent normal tissue and compared with their counterparts from normal bone using a set of macrophage polarization markers, including CD204, CD206, CD86, CD64, MHCII, and IL4R, indicated that all three macrophage populations have heterogeneous expression of these markers (Fig. 3 D). BoMAMs have higher IL4R expression and increased abundance of $CD204^+$ cells (Fig. 3 D). Multiparameter FACS analysis indicated that IL4R and CD204 colocalize and label a distinct population of macrophages that are specific for bone metastasis (Fig. 3 E). Immunofluorescent staining further confirmed that CD204 staining specifically labeled macrophages that infiltrate inside the bone metastasis, and that they have relatively low F4/80 expression compared with the macrophages in adjacent normal bone marrow (peritumor; Fig. 3 F). These $CD204^+$ macrophages consistently coexpress IL4R and the lineage marker Iba1, as assessed by double immunofluorescent staining (Fig. 3 G). Importantly, in patient bone metastases samples, $CD204^+$ macrophages infiltrated into the tumor in all the cases in our cohort, and the majority of these macrophages also expressed IL4R (Fig. 4 A). Furthermore, in two independent breast cancer bone metastasis datasets, CD204 expression was strongly correlated with a macrophage IL4R target gene score (Palazon et al., 2017; Zhang et al., 2009; Fig. 4 B). Together, these data strongly suggest that IL4R signaling in macrophages plays an important role in breast cancer bone metastasis.

Monocyte-derived macrophage promotion of bone metastasis is IL4R dependent

$Ly6C^+CCR2^+$ monocytes are mostly $CD204^+$ in both healthy and bone metastasis–bearing mice (Fig. 5 A), and bone metastasis–associated monocytes have significantly higher IL4R expression compared with normal counterparts in gene expression profile analysis (Fig. 5 B). Because our data indicate that $Ly6C^+$ IM recruitment is enhanced in bone metastasis (Fig. 2 B), we hypothesized that $CD204^+IL4R^+$ BoMAMs are mainly derived from IMs. To test this directly, we performed lineage tracing experiments using adoptive transfer of $Ly6C^+$ monocytes FACS sorted from ubiquitous GFP-expressing mice (FVB.Cg-Tg(CAG-EGFP)B5Nagy/J) into syngeneic mice bearing established bone metastasis and recovered GFP^+ cells for immunophenotyping (Fig. 5 C, left). Compared with endogenous macrophages (GFP^-), monocyte-derived macrophages (GFP^+) almost exclusively expressed both CD204 and IL4R and represented tumor-infiltrating BoMAMs, whereas the endogenous macrophages (GFP^-) were largely $IL4R^-$ and had dichotomized expression of CD204 that was consistent with data in Fig. 3 A (Fig. 5 C). These data directly indicate that the majority of $IL4R^+$ BoMAMs are derived from recruited IMs.

IL4R has been shown to have multiple functions in different cell types including macrophages, T and B lymphocytes, and nonhematopoietic cells (Ho and Miaw, 2016). To test the role of macrophage IL4R in bone metastasis, we crossed $Il4ra^{-/-}$ mice (Mohrs et al., 1999) with $Rag2^{-/-}$ mice that lack mature T and B cells. These mice were then used as bone marrow donors to generate mosaic mice in lethally irradiated *Foxn1* nude mice. As a result, these mosaic mice lack mature T and B function, and the IL4R deficiency is limited to bone marrow–derived innate immune cells, predominantly macrophages. The bone colonization potential of 1833 cells was significantly inhibited in mosaic mice bearing $Il4ra^{-/-}$ bone marrow compared with control mosaic mice containing $Il4ra^{+/-}$ bone marrow (Fig. 5 D). Furthermore, osteoclast abundance in $IL4R^{-/-}$ bone marrow mosaic mice was comparable with that in control mice with $Il4ra^{+/-}$ bone marrow (Fig. S5 A). In contrast, abundance of $CD204^+$ BoMAMs was significantly reduced (Fig. S5 B). This suggests that IL4R is important for activation of BoMAMs but not osteoclasts.

Additional experiments were performed to determine *Il4* mRNA expression using quantitative PCR on various cell types purified from the bone metastasis environment by FACS sorting. Our data indicate that $CD4^+$ T cells have the highest *Il4* expression; tumor cells and B cells also have some *Il4* mRNA expression; and all other cells type tested did not have detectable *Il4* expression. (Fig. S5 C). This suggests paracrine signaling between $CD4^+$ T cells and BoMAMs through IL-4, which is consistent with previous studies in primary breast cancer models (DeNardo et al., 2009).

Our data indicate that BoMAMs are derived from $Ly6C^+$ IMs. The abundance of monocytes and macrophages in $Il4ra^{-/-}$ bone marrow mosaic mice is similar to $Il4ra^{+/-}$ controls with comparable bone metastasis burden (Fig. S5 B). This suggests that IL4R mainly affects BoMAM tumor-promoting function rather than recruitment. Indeed, in similar monocyte add-back experiments as described in Fig. 2 H, $IL4R^{-/-}$ monocytes were less efficient at promoting bone metastasis growth compared with $IL4R^{+/+}$ monocytes, despite equivalent recruitment (Fig. 5 E). Together, these data indicated that macrophage IL4R signaling is critical for BoMAM activation and tumor-promoting function.

Discussion

Compelling evidence indicates that macrophages play important roles in cancer metastatic progression and that targeting macrophages could have significant therapeutic benefit (Cassetta and Pollard, 2018; Quail and Joyce, 2017; Ruffell and Coussens, 2015). However, metastasis still remains a major cause of death. In particular, in breast and other cancers, outgrowth of bone metastasis represent a major clinical challenge (Mundy, 2002). The current study provides direct evidence that macrophages

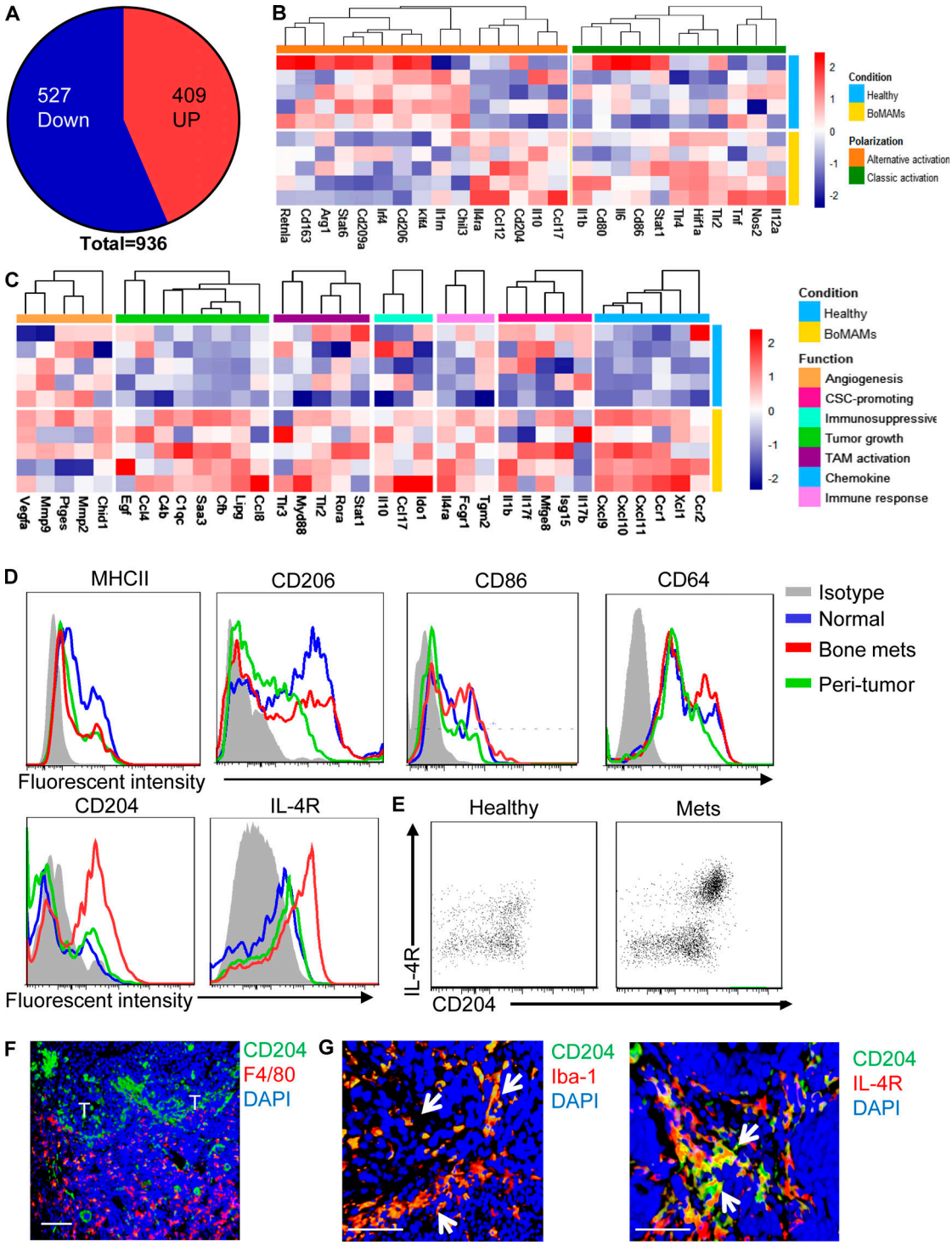

Figure 3. **BoMAMs bear distinct cell surface markers. (A)** Pie chart of the total number of differentially expressed genes that are up-regulated or down-regulated in macrophages associated with bone metastasis compared with macrophages from normal bone. Differentially expressed genes are defined as fold-change >1.5, $P < 0.05$. **(B)** Heatmap showing the expression of major macrophage polarization markers. Bar denotes the relative expression level of each gene in each sample. **(C)** Heatmap showing the expression of genes of major tumor-promoting functions. Bar denotes the relative expression level of each gene in each sample. CSC, cancer stem cell; TAM, tumor-associated macrophage. **(D)** Representative histogram of different macrophage markers determined by flow cytometry in bone marrow macrophages from healthy mice (blue), bone metastasis (red), and adjacent normal (peritumor; green). Gray represents isotype control. Experiments performed three times independently. **(E)** Representative flow dot plot of CD204 and IL-4R (CD124) expression in macrophages from healthy bone marrow and BoMaMs. Experiments performed three times independently. **(F)** Representative immunofluorescent staining of CD204 and F4/80 in MetBo2 bone metastasis and adjacent normal bone marrow. Bar = 50 µm. T, tumor area. Experiments performed three times independently. **(G)** Representative immunofluorescent staining of CD204$^+$ macrophage populations coexpressing Iba-1 and IL-4R in bone metastasis. Bar = 20 µm. Arrows point to the coexpression of markers (yellow) on macrophages. Experiments performed three times independently.

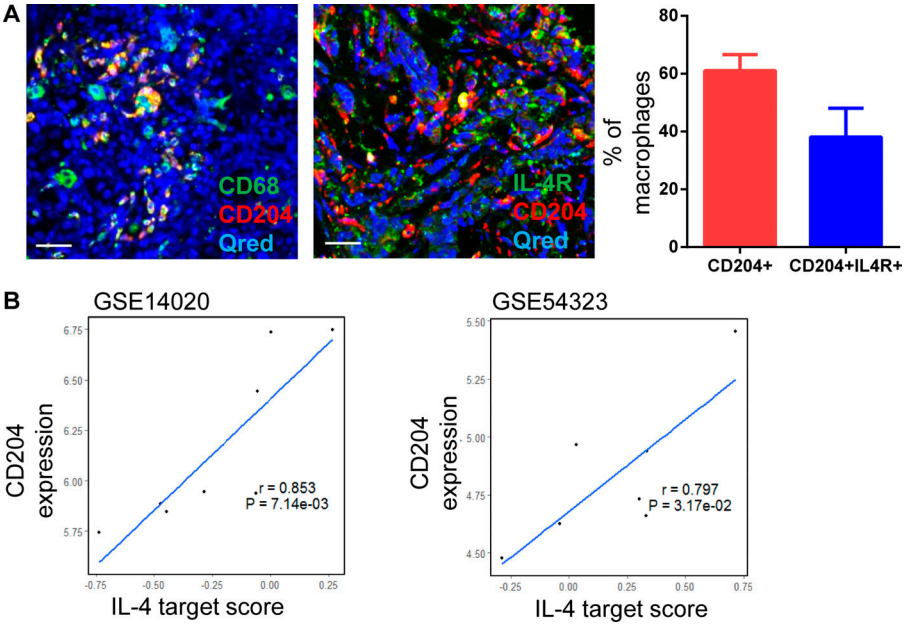

Figure 4. **BoMAMs in human samples. (A)** Multiplex immunofluorescent staining of CD204 and IL4R macrophages in patient breast cancer bone metastasis (bar = 20 µm) and quantification (n = 9 samples; error bar represents SEM). **(B)** IL4 target score correlation with CD204 expression in patient bone metastasis transcriptome datasets. Each point represents a patient sample in the dataset.

are critical for breast cancer bone outgrowth. Macrophage ablation or inhibition of CSF1 receptor potently inhibited bone metastasis outgrowth of both mouse and human breast cancer cells in immune-competent and -deficient mice, respectively. These data suggest that macrophage targeting might be an effective therapeutic approach in treating breast cancer bone disease.

Macrophages can be derived from embryonic precursor cells and bone marrow monocytes (Jacome-Galarza et al., 2019). In the current study, our data strongly suggest that monocyte-derived BoMAMs are critical for bone metastasis outgrowth in an IL4R-dependent manner. BoMAMs express low levels of F4/80 in immunofluorescent staining, which is one of the characteristics of monocyte-derived macrophages (Schulz et al., 2012). Consistent with this data, a deficiency in CCR2-dependent monocyte recruitment significantly inhibited bone colonization efficiency, while the add-back of WT monocytes restored bone metastasis outgrowth. Embryonic precursor cells give rise to tissue-resident macrophages in almost all tissues (Perdiguero and Geissmann, 2016). Studies by Frenette's group and others suggest that $CD169^+$ macrophages represent such bone-resident macrophages, and that these control the perivascular hematopoietic stem cell niche (Chow et al., 2013). In the current study, depletion of these macrophages using CD169-DTR mice did not affect metastasis outgrowth. Consistent with this result, we found that the majority of the resident macrophages do not express IL4R, a receptor that is critical for bone metastasis outgrowth. Together with the data from $Ccr2^{-/-}$ mice and the monocyte add-back rescue experiments, this indicates that, at least in the models tested here, bone metastasis–promoting macrophages are predominantly derived from recruited IMs. Interestingly, the contribution of tissue-resident macrophages can vary among different secondary organs and cancer types. For example, resident macrophages have been shown to play an important role in tumor progression of primary pancreatic adenocarcinomas (Zhu et al., 2017). Therefore, distinct macrophage subsets may play dominant roles in different cancer types and different secondary organs. This suggests the need for precisely targeted therapies to maximize patient benefit.

It is interesting that adoptive transfer of WT IMs, but not $Ccr2^{-/-}$ counterparts, can significantly promote bone metastasis growth in $Ccr2^{-/-}$ mice. These data suggest that CCR2-dependent monocyte recruitment is critical for bone metastasis outgrowth. Our previous studies showed a similar mechanism of monocytes in promotion of breast cancer lung metastasis seeding and extravasation (Qian et al., 2011). In both cases, tissue-resident macrophages did not seem to play major tumor supporting roles. Interestingly, Kuffer cell and microglia, tissue-resident macrophages of liver and brain respectively, have been shown to play important roles in the process of breast cancer metastasis to these two target organs (Bowman et al., 2016; Gordon et al., 2017; Hoshino et al., 2015; Zhu et al., 2017). Together, these data underline macrophage heterogeneity as an important component of tissue microenvironment (the "soil") that determines tissue-specific metastatic mechanisms. Of note, the CCL2/CCR2 axis may also regulate the phenotype (Sierra-Filardi et al., 2014) or function of macrophages, as has been shown in melanoma, lung, and liver cancer models (Kitamura et al., 2015a; Li et al., 2017; Xu et al., 2019). Our data cannot exclude the possibility that a similar mechanism may also exist in breast cancer bone metastasis after the recruitment of IMs.

IL4R has been shown to induce alternative activation of macrophages (Varin et al., 2010), Ig production in B cells (Yanagihara et al., 1995), activation of type 2 T helper cells, and signaling in nonhematopoietic cells (Li et al., 2009). Previous studies have illustrated the role of IL4/IL4R signaling in tumor invasion and response to treatment in primary breast cancer (Andreu et al., 2010; Venmar et al., 2014) and glioma models (Pyonteck et al., 2013). The current study revealed that IL4R signaling is critical for the polarization and protumor function of BoMAMs. Together, these data suggest that the IL4/IL4R pathway can be a promising target in neutralizing tumor-promoting macrophages.

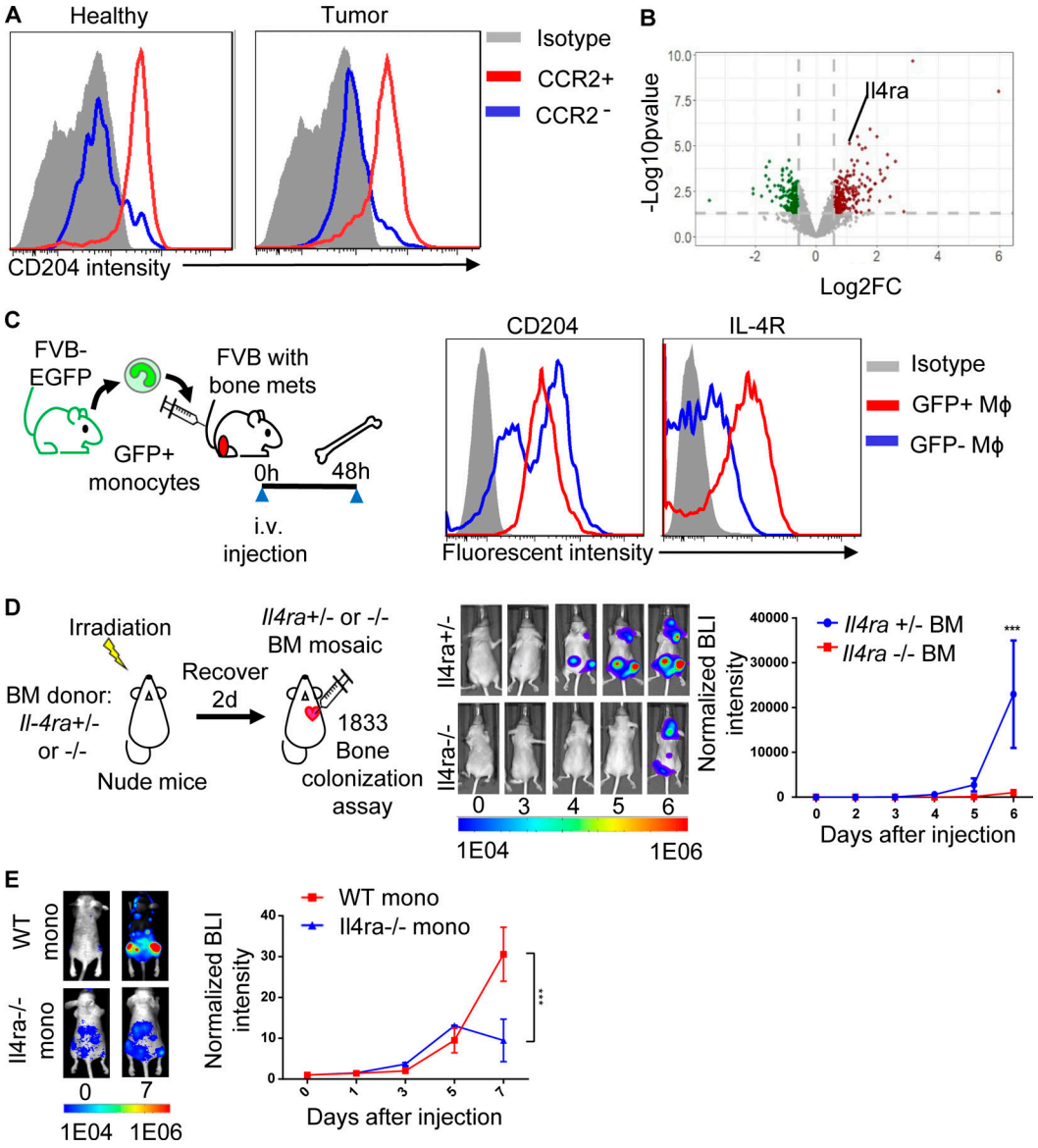

Figure 5. **Monocyte-derived macrophage promotion of bone metastasis is IL4R dependent. (A)** CD204 expression of CCR2⁺ and CCR2⁻ monocytes from healthy control and bone metastasis. Gray, isotype control; red, CCR2⁺ monocytes; blue, CCR2⁻ monocytes. *n* = 3. Experiments performed two times independently. **(B)** Volcano plot showing that Il4ra is highly up-regulated in monocytes from MetBo2 bone metastases compared with monocytes sorted from healthy mice. Volcano plot showing −log10(P value) versus log2(fold-change). Red colored points represent up-regulated gene with P < 0.05 and fold-change >1.5; green colored points represent down-regulated gene with P < 0.05 and fold-change >1.5. **(C)** Diagram of GFP⁺ monocyte adoptive transfer into bone metastasis (mets) bearing syngeneic host (left) and representative FACS histogram (right) showing CD204 and IL4R expression comparing monocyte-derived macrophages (GFP⁺) and endogenous macrophages (GFP⁻). Gray, isotype control; red, GFP⁺ macrophages; blue, GFP⁻ macrophages. *n* = 3. Experiments performed two times independently. **(D)** Diagram of bone colonization assay in mosaic mice bearing *Il4r*$^{+/-}$ and *Il4r*$^{-/-}$ bone marrow (left). Representative images and quantification of bioluminescent (BLI) signal of 1833 bone metastasis in bone marrow (BM) mosaic mice generated as described in the diagram (right). Signals were measured by IVIS and normalized to day 0. *n* = 10 for each group. Bar represents SEM. ***, P < 0.001 with Student's *t* test. Experiments performed two times independently. **(E)** Representative images and quantification of bioluminescent signal of 1833 bone metastasis in mice adoptively transferred with WT or *Il4r*$^{-/-}$ monocytes. Signals were quantified by PhotonIMAGER and normalized to day 0. *n* = 3–5. Bar represents SEM. Each group contain data from four legs. Bar represents SEM. ***, P < 0.001 with Student's *t* test. Experiments performed three times independently.

In summary, we have elucidated a novel mechanism that promotes breast cancer bone metastasis outgrowth through a specific subset of CD204⁺IL4R⁺ macrophages derived from CCR2-recruited IMs. This population of BoMAMs is preserved in patient bone metastasis samples. This mechanism can be potentially targeted to treat breast cancer bone disease.

Material and methods

Animal studies

All animal procedures were performed based on the UK Animals Act 1986 following local rules and approved project license or in accordance with National Institutes of Health regulations concerning the use and care of experimental animals, with approval by the Albert Einstein College of Medicine Animal Use Committee.

FVB/N, athymic nude (outbreed, mixed background) and albino-b6 mice were bought from Charles River. B6.129S4-Ccr2tm1Ifc/J (*Ccr2*$^{-/-}$), B6.Il4ratm1Sz/J(*Il4ra*$^{-/-}$), B6(Cg)-Rag2tm1.1Cgn/J (*Rag2*$^{-/-}$), and FVB.Cg-Tg(CAG-EGFP)B5Nagy/J (FVB-eGFP) mice were bought from Jackson Laboratory. CD169-DTR mice were kindly provided by Prof. Paul Frenette (Albert Einstein College of Medicine, New York, NY). *Csf1r-EGFP* (MacGreen) mice on the C57BL/6 background were obtained from Dr. David Hume (University of Edinburgh, Edinburgh, UK). *Ccr2*$^{-/-}$ mice and CD169-DTR mice were crossed with athymic mice. *Il4ra*$^{-/-}$ mice were crossed with *Rag2*$^{-/-}$ mice. For generation of bone marrow mosaic mice, recipient mice received 8 Gy irradiation at the age of 3 wk and rested for 5 h before an i.v. injection of bone marrow cells from donor mice. The mice were allowed to recover for 3 wk before metastasis assays were performed. All the in vivo experiments were repeated at least twice with more than three mice in each group.

Human tissue and multiplex immunofluorescent staining

The bone metastases samples were collected from nine patients diagnosed with grade IV breast cancer from 2016 to 2017. This study followed standard guidelines and was approved by the Ethics Committee of the Second Affiliated Hospital of Zhejiang University School of Medicine, Hangzhou, China. Written informed consent was obtained from all participants. Multiplex staining was performed with slides cut from formalin-fixed and paraffin-embedded patient bone metastasis samples. Their demographic information, including sex, sampling site, and molecular phenotype, is shown in Table S1. For PanCK staining, slides were retrieved in 0.125 mM EDTA solution (pH 8.0) at 97°C for 45 min in a pressure cooker. After cooling, samples were incubated in 30% vol/vol hydrogen peroxide for 30 min and blocked. Staining was performed using Alexa Fluor 488 Tyramide SuperBoost Kit (Thermo Fisher Scientific; B40941) via the protocol recommended by the antibody providers. For multiplexing staining, the method described previously was used (Prost et al., 2016) with protocols provided by the manufacturer. Anti-human primary antibodies used were PanCK (AE1/AE3, Thermo Fisher Scientific), CD204 (Abnova; SRA-E5), CD68 (Dako; PG-M1), and IL-4Ra (R&D Systems; MAB230). Other products used were serum-free block (Dako; X0909), Qred (1/750, Thermo Fisher Scientific; Q10363), Avidin/Biotin blocking kit (Vector; SP-2001), and EcoMount (Biocare Medical; EM897L). Samples were scanned and unmixed using Polariz multispectral slide scanner (Vectra) and analyzed using Nuance.

Mouse tissue

Mouse bone metastasis samples were fixed by 4% wt/vol paraformaldehyde for 30 min, incubated with 30% wt/vol sucrose overnight, and embedded in optimal cutting temperature compound at −20°C. Then bone was shaved to expose bone marrow, washed in PBS, and blocked with 5% wt/vol BSA and anti-mouse CD16/32 antibody (BD Biosciences; 1:200). Primary and secondary antibodies were stained in the dark. The bone was imaged by spinning-disk confocal microscopy. 3D images were generated via Volocity. FACS antibodies as described below and anti-Iba1 (WDR2342) were used for staining. Tartrate-resistant acid phosphatase (TRAP) staining was performed for osteoclast quantification. An Acid Phosphatase, Leukocyte (TRAP) Kit (Sigma-Aldrich) was used based on manufacturer's guidelines. Imaging was performed with Axioskop 2 (Zeiss).

Cell culture

MetBo2 is an in house–selected bone homing clone of the mouse breast cancer cell line Met-1, which was derived from polyoma middle T oncogene tumor as previously described (Qian et al., 2009). Human breast cancer cell line 1833 (bone metastatic clone of triple-negative breast cancer cell line MDA-MB-231) was a gift from Prof. Joan Massagué (Memorial Sloan Kettering Cancer Center, New York, NY). Cells were cultured in DMEM (Gibco) supplemented with 10% vol/vol heat-inactivated FBS (Gibco) and 1% vol/vol penicillin-streptomycin (Gibco). Cells were maintained at 37°C with 5% vol/vol CO_2 in an incubator. All cells were negative for mycoplasma (Applied Biological Materials Inc.). Short tandem repeat tests were performed for human cells to make sure of their authenticity.

Experimental metastasis assay and treatment

Bone metastasis was generated through intracardiac injection of 10^5 tumor cells into 4-wk-old female mice of strains described above. Bioluminescent signal was recorded twice a week using the Photon IMAGER Optima system (Biospace) or IVIS spectrum (PerkinElmer). The region of interest was quantified by Photon IMAGER software or IVIS Living Imaging v4.3.1. Macrophage depletion was performed by i.v. injection of liposome-encapsulated clodronate (1 mg/mouse; Liposoma) twice a week. BLZ945 was given as daily gavage (200 mg/kg body weight; MedChemExpress). CCL2-neutralizing antibody or the control antibody (20 mg/kg body weight; Ortho BiotechOncology) was administered twice a week. Osteoclast depletion was performed by i.p. injections of free clodronate (dichloromethylenediphosphonic acid disodium salt; Sigma-Aldrich; 1 mg/mouse) on day 0, day 1, and then twice a week after tumor was detected.

For adoptive transfer, 1 × 10^6 monocytes (CD45$^+$CD11b$^+$CSF1R$^+$Ly6C$^+$) from the bone of WT, *Ccr2*$^{-/-}$, or *Il4ra*$^{-/-}$ were sorted and injected via intracaudal injection to mice with detectable bone metastasis. Mice were imaged right before monocyte transfer and on day 1, 3, 7, and 10 for quantification of tumor growth. For lineage tracking, 1 × 10^6 GFP$^+$ monocytes (from FVB-eGFP or *Csf1r-EGFP* mice) were injected i.v. into mice with late-stage bone metastasis. Bone and blood were collected 48 h after injection.

FACS analysis

For mice with bone metastasis, bone was separated into tumor and peritumor areas based on the bioluminescent signal. Samples were then digested in DMEM supplemented with Librease TL, Librease DL, DNase I, and hyaluronidase (1:100 each) on a shaker at 37°C for 30 min. Blood was drawn by cardiac puncture with heparin (Sigma-Aldrich). Spleen was mashed using the plunger from an insulin syringe into a 40-µM cell strainer (Falcon). Red blood cell lysis buffer (eBioscience) was used to remove red blood cells. Cells were blocked with anti-mouse CD16/32 antibody (BD Biosciences; 1:500) before staining.

Surface markers were stained for 30 min on ice and washed with PBS. Cells were sorted on Aria II or Fusion or analyzed on Fortessa (BD Bioscience). Antibodies used were as follows: CD11b (M1/70), Ly6G (1A8), Ly6C (HK1.4), F4/80 (BM8), CCR2 (FAB5538A), CD45 (30-F11), CD64(X54-5/7.1), CD86 (GL-1), CD115 (AFS98), CD169 (SER-4), CD206 (C068C2), MHCII (M5/114.15.2), MSR-1 (FAB1797P), mouse IgG1 (MOPC-21), rat IgG2a (RTK2758), hamster IgG (HTK888), B220 (RA3-6B2), CD3 (17A2), CD4 (RM4-5), CD8a (53–6.7), CD19 (6D5), and NK1.1 (PK136).

FACS sorting and gene expression array analysis

Tissue preparation and antibodies were the same as those described in FACS analysis. Inflammatory monocytes (Ly6C$^+$) were sorted from bones bearing metBo2 or healthy controls. Total RNA was extracted from these sorted macrophages (RNeasy Mini kit; Qiagen), and its quality was determined using Pico Chip with a 2100 Bioanalyzer (Agilent Technologies). Samples where then submitted to the Albert Einstein College of Medicine microarray facility for labeling and hybridization on Affymetrix MoGene 2.0 ST chips. Differential gene expression analysis was performed using R package limma (Ritchie et al., 2015). Genes with fold-change more than ±1.5 and $P < 0.05$ were considered differentially expressed. Original data were deposited in the Gene Expression Omnibus (accession no. GSE152795).

Quantitative real-time PCR

Immune cell populations and tumor cells were sorted from MetBo2 bone metastasis samples. RNA was extracted by RNeasy Plus Micro Kit (Qiagen). Primers were Il4ra forward, 5′-TGTGCC AAACGTCCTCACAGCA-3′, and reverse, 5′-TCCAGGCATCGA AAAGCCCGAA-3′.

Bioinformatics

Bioinformatics analysis was performed with R and Bioconductor. Gene annotation was performed using the Database for Annotation, Visualization, and Integrated Discovery. For correlation analysis, three individual datasets with breast cancer bone metastasis samples (GSE14020 and GSE54323) were used. IL4 target score was calculated using differentially regulated genes in IL4-treated macrophages reported by Gupta et al. (2018) and single-sample gene set enrichment analysis (Barbie et al., 2009) and the gene set variation analysis package (GSVA; Hänzelmann et al., 2013). Pearson correlation analysis was used to analyze the correlation between IL4 target scores and IL4R and CD204 expression.

Statistical analysis

Statistical analysis was performed with GraphPad Prism (v7). Two-tailed Student's *t* test and ANOVA followed by multiple comparison was used to calculate statistical significance. The difference was considered significant with a P value <0.05.

Online supplemental material

Fig. S1 indicates that macrophage depletion assays specifically ablate macrophages but do not affect other bone marrow immune cells, and neither assay affects the growth of abdominal metastasis. Fig. S2 demonstrates that L-Clod depletes both bone marrow macrophages and osteoclasts, showing a better inhibition of bone metastasis growth than osteoclast-specific depletion. Fig. S3 shows that CD169$^+$ bone-resident macrophages do not play a predominant role in breast cancer bone metastasis outgrowth. Fig. S4 demonstrates that the deficiency of *Ccr2* leads to a significant reduction of IMs in blood but does not affect monocyte populations in bone marrow. Fig. S5 indicates that *Il4ra* deficiency specifically affects CD204$^+$ BoMAMs in the 1833 bone metastasis model. Also, IL-4 is produced by T cells, B cells, and tumor cells in bone metastasis. Table S1 shows clinical information for breast cancer bone patients.

Acknowledgments

This work was supported by Cancer Research UK Career Development Fellowship C49791/A17367, European Research Council starting grant 716379to B.-Z. Qian; National Natural Science Foundation of China grant 81872150; National Cancer Institute cancer grants P30CA013330 and RO1CA131270 and Wellcome Trust grant 101067/Z/13/Z to J.W. Pollard; and an Edinburgh Global Research scholarship to R.-Y. Ma. This work was undertaken in the Medical Research Council Centre for Reproductive Health, which is funded by Medical Research Council Centre grant MR/N022556/1.

Author contributions: B.-Z. Qian and R.-Y. Ma designed the experiments and wrote the manuscript. R.-Y. Ma, H. Zhang, X.-F. Li, and A.D. Lam performed animal experiments. C.-B. Zhang, G. Tagliavini, S. Prost, and Z. Wang helped with tissue staining. C. Selli and A.H. Sims contributed to the bioinformatics analysis. Z. Ye, H.-Y. Hu, and T. Ying provided human samples or materials used in this study. J.W. Pollard and B.-Z. Qian supervised this project. All authors reviewed and approved the manuscript.

Disclosures: J.W. Pollard is the co-founder of Macomics, a start-up immunooncology company. The company is not yet trading, and there are no conflicts between this company and the data in the current paper. No other disclosures were reported.

Submitted: 27 September 2019
Revised: 8 April 2020
Accepted: 23 June 2020

References

Afik, R., E. Zigmond, M. Vugman, M. Klepfish, E. Shimshoni, M. Pasmanik-Chor, A. Shenoy, E. Bassat, Z. Halpern, T. Geiger, et al. 2016. Tumor macrophages are pivotal constructors of tumor collagenous matrix. *J. Exp. Med.* 213:2315–2331. https://doi.org/10.1084/jem.20151193

Andreu, P., M. Johansson, N.I. Affara, F. Pucci, T. Tan, S. Junankar, L. Korets, J. Lam, D. Tawfik, D.G. DeNardo, et al. 2010. FcRgamma activation regulates inflammation-associated squamous carcinogenesis. *Cancer Cell.* 17:121–134. https://doi.org/10.1016/j.ccr.2009.12.019

Auffray, C., M.H. Sieweke, and F. Geissmann. 2009. Blood monocytes: development, heterogeneity, and relationship with dendritic cells. *Annu. Rev. Immunol.* 27:669–692. https://doi.org/10.1146/annurev.immunol.021908.132557

Barbie, D.A., P. Tamayo, J.S. Boehm, S.Y. Kim, S.E. Moody, I.F. Dunn, A.C. Schinzel, P. Sandy, E. Meylan, C. Scholl, et al. 2009. Systematic RNA interference reveals that oncogenic KRAS-driven cancers require TBK1. *Nature.* 462:108–112. https://doi.org/10.1038/nature08460

Batoon, L., S.M. Millard, M.E. Wullschleger, C. Preda, A.C. Wu, S. Kaur, H.W. Tseng, D.A. Hume, J.P. Levesque, L.J. Raggatt, et al. 2019. CD169^{+} macrophages are critical for osteoblast maintenance and promote intramembranous and endochondral ossification during bone repair. *Biomaterials*. 196:51–66. https://doi.org/10.1016/j.biomaterials.2017.10.033

Bowman, R.L., F. Klemm, L. Akkari, S.M. Pyonteck, L. Sevenich, D.F. Quail, S. Dhara, K. Simpson, E.E. Gardner, C.A. Iacobuzio-Donahue, et al. 2016. Macrophage Ontogeny Underlies Differences in Tumor-Specific Education in Brain Malignancies. *Cell Rep*. 17:2445–2459. https://doi.org/10.1016/j.celrep.2016.10.052

Cassetta, L., and J.W. Pollard. 2018. Targeting macrophages: therapeutic approaches in cancer. *Nat. Rev. Drug Discov*. 17:887–904. https://doi.org/10.1038/nrd.2018.169

Cassetta, L., S. Fragkogianni, A.H. Sims, A. Swierczak, L.M. Forrester, H. Zhang, D.Y.H. Soong, T. Cotechini, P. Anur, E.Y. Lin, et al. 2019. Human Tumor-Associated Macrophage and Monocyte Transcriptional Landscapes Reveal Cancer-Specific Reprogramming, Biomarkers, and Therapeutic Targets. *Cancer Cell*. 35:588–602.e10. https://doi.org/10.1016/j.ccell.2019.02.009

Chow, A., M. Huggins, J. Ahmed, D. Hashimoto, D. Lucas, Y. Kunisaki, S. Pinho, M. Leboeuf, C. Noizat, N. van Rooijen, et al. 2013. CD169^{+} macrophages provide a niche promoting erythropoiesis under homeostasis and stress. *Nat. Med*. 19:429–436. https://doi.org/10.1038/nm.3057

Chow, A., D. Lucas, A. Hidalgo, S. Méndez-Ferrer, D. Hashimoto, C. Scheiermann, M. Battista, M. Leboeuf, C. Prophete, N. van Rooijen, et al. 2011. Bone marrow CD169+ macrophages promote the retention of hematopoietic stem and progenitor cells in the mesenchymal stem cell niche. *J. Exp. Med*. 208:261–271. https://doi.org/10.1084/jem.20101688

Coleman, R.E.. 2001. Metastatic bone disease: clinical features, pathophysiology and treatment strategies. *Cancer Treat. Rev*. 27:165–176. https://doi.org/10.1053/ctrv.2000.0210

Coleman, R.E.. 2006. Clinical features of metastatic bone disease and risk of skeletal morbidity. *Clin. Cancer Res*. 12:6243s–6249s. https://doi.org/10.1158/1078-0432.CCR-06-0931

DeNardo, D.G., J.B. Barreto, P. Andreu, L. Vasquez, D. Tawfik, N. Kolhatkar, and L.M. Coussens. 2009. CD4(+) T cells regulate pulmonary metastasis of mammary carcinomas by enhancing protumor properties of macrophages. *Cancer Cell*. 16:91–102. https://doi.org/10.1016/j.ccr.2009.06.018

Franklin, R.A., W. Liao, A. Sarkar, M.V. Kim, M.R. Bivona, K. Liu, E.G. Pamer, and M.O. Li. 2014. The cellular and molecular origin of tumor-associated macrophages. *Science*. 344:921–925. https://doi.org/10.1126/science.1252510

Geissmann, F., M.G. Manz, S. Jung, M.H. Sieweke, M. Merad, and K. Ley. 2010. Development of monocytes, macrophages, and dendritic cells. *Science*. 327:656–661. https://doi.org/10.1126/science.1178331

Getts, D.R., R.L. Terry, M.T. Getts, M. Müller, S. Rana, B. Shrestha, J. Radford, N. Van Rooijen, I.L. Campbell, and N.J. King. 2008. Ly6c+ "inflammatory monocytes" are microglial precursors recruited in a pathogenic manner in West Nile virus encephalitis. *J. Exp. Med*. 205:2319–2337. https://doi.org/10.1084/jem.20080421

Gordon, S., and A. Plüddemann. 2019. The Mononuclear Phagocytic System. Generation of Diversity. *Front. Immunol*. 10:1893. https://doi.org/10.3389/fimmu.2019.01893

Gordon, S.R., R.L. Maute, B.W. Dulken, G. Hutter, B.M. George, M.N. McCracken, R. Gupta, J.M. Tsai, R. Sinha, D. Corey, et al. 2017. PD-1 expression by tumour-associated macrophages inhibits phagocytosis and tumour immunity. *Nature*. 545:495–499. https://doi.org/10.1038/nature22396

Gupta, S., A. Jain, S.N. Syed, R.G. Snodgrass, B. Pflüger-Müller, M.S. Leisegang, A. Weigert, R.P. Brandes, I. Ebersberger, B. Brüne, et al. 2018. IL-6 augments IL-4-induced polarization of primary human macrophages through synergy of STAT3, STAT6 and BATF transcription factors. *OncoImmunology*. 7. e1494110. https://doi.org/10.1080/2162402X.2018.1494110

Hänzelmann, S., R. Castelo, and J. Guinney. 2013. GSVA: gene set variation analysis for microarray and RNA-seq data. *BMC Bioinformatics*. 14:7. https://doi.org/10.1186/1471-2105-14-7

Hashimoto, D., A. Chow, C. Noizat, P. Teo, M.B. Beasley, M. Leboeuf, C.D. Becker, P. See, J. Price, D. Lucas, et al. 2013. Tissue-resident macrophages self-maintain locally throughout adult life with minimal contribution from circulating monocytes. *Immunity*. 38:792–804. https://doi.org/10.1016/j.immuni.2013.04.004

Ho, I.-C., and S.-C. Miaw. 2016. Regulation of IL-4 Expression in Immunity and Diseases. *In* Regulation of Cytokine Gene Expression in Immunity and Diseases. X. Ma, editor. Springer Netherlands, Dordrecht. pp. 31–77. https://doi.org/10.1007/978-94-024-0921-5_3

Hoshino, A., B. Costa-Silva, T.L. Shen, G. Rodrigues, A. Hashimoto, M. Tesic Mark, H. Molina, S. Kohsaka, A. Di Giannatale, S. Ceder, et al. 2015. Tumour exosome integrins determine organotropic metastasis. *Nature*. 527:329–335. https://doi.org/10.1038/nature15756

Jacome-Galarza, C.E., G.I. Percin, J.T. Muller, E. Mass, T. Lazarov, J. Eitler, M. Rauner, V.K. Yadav, L. Crozet, M. Bohm, et al. 2019. Developmental origin, functional maintenance and genetic rescue of osteoclasts. *Nature*. 568:541–545. https://doi.org/10.1038/s41586-019-1105-7

Kang, Y., P.M. Siegel, W. Shu, M. Drobnjak, S.M. Kakonen, C. Cordón-Cardo, T.A. Guise, and J. Massagué. 2003. A multigenic program mediating breast cancer metastasis to bone. *Cancer Cell*. 3:537–549. https://doi.org/10.1016/S1535-6108(03)00132-6

Kitamura, T., B.Z. Qian, and J.W. Pollard. 2015a. Immune cell promotion of metastasis. *Nat. Rev. Immunol*. 15:73–86. https://doi.org/10.1038/nri3789

Kitamura, T., B.Z. Qian, D. Soong, L. Cassetta, R. Noy, G. Sugano, Y. Kato, J. Li, and J.W. Pollard. 2015b. CCL2-induced chemokine cascade promotes breast cancer metastasis by enhancing retention of metastasis-associated macrophages. *J. Exp. Med*. 212:1043–1059. https://doi.org/10.1084/jem.20141836

Li, X., W. Yao, Y. Yuan, P. Chen, B. Li, J. Li, R. Chu, H. Song, D. Xie, X. Jiang, et al. 2017. Targeting of tumour-infiltrating macrophages via CCL2/CCR2 signalling as a therapeutic strategy against hepatocellular carcinoma. *Gut*. 66:157–167. https://doi.org/10.1136/gutjnl-2015-310514

Li, Z., L. Chen, and Z. Qin. 2009. Paradoxical roles of IL-4 in tumor immunity. *Cell. Mol. Immunol*. 6:415–422. https://doi.org/10.1038/cmi.2009.53

Lin, E.Y., A.V. Nguyen, R.G. Russell, and J.W. Pollard. 2001. Colony-stimulating factor 1 promotes progression of mammary tumors to malignancy. *J. Exp. Med*. 193:727–740. https://doi.org/10.1084/jem.193.6.727

Liu, H., J. He, S.P. Koh, Y. Zhong, Z. Liu, Z. Wang, Y. Zhang, Z. Li, B.T. Tam, P. Lin, et al. 2019. Reprogrammed marrow adipocytes contribute to myeloma-induced bone disease. *Sci. Transl. Med*. 11. eaau9087. https://doi.org/10.1126/scitranslmed.aau9087

Maurizi, A., and N. Rucci. 2018. The Osteoclast in Bone Metastasis: Player and Target. *Cancers (Basel)*. 10:218. https://doi.org/10.3390/cancers10070218

Mohrs, M., B. Ledermann, G. Köhler, A. Dorfmüller, A. Gessner, and F. Brombacher. 1999. Differences between IL-4- and IL-4 receptor α-deficient mice in chronic leishmaniasis reveal a protective role for IL-13 receptor signaling. *J. Immunol*. 162:7302–7308.

Mundy, G.R.. 2002. Metastasis to bone: causes, consequences and therapeutic opportunities. *Nat. Rev. Cancer*. 2:584–593. https://doi.org/10.1038/nrc867

Ojalvo, L.S., W. King, D. Cox, and J.W. Pollard. 2009. High-density gene expression analysis of tumor-associated macrophages from mouse mammary tumors. *Am. J. Pathol*. 174:1048–1064. https://doi.org/10.2353/ajpath.2009.080676

Palazon, A., P.A. Tyrakis, D. Macias, P. Veliça, H. Rundqvist, S. Fitzpatrick, N. Vojnovic, A.T. Phan, N. Loman, I. Hedenfalk, et al. 2017. An HIF-1α/VEGF-A Axis in Cytotoxic T Cells Regulates Tumor Progression. *Cancer Cell*. 32:669–683.e5. https://doi.org/10.1016/j.ccell.2017.10.003

Palframan, R.T., S. Jung, G. Cheng, W. Weninger, Y. Luo, M. Dorf, D.R. Littman, B.J. Rollins, H. Zweerink, A. Rot, et al. 2001. Inflammatory chemokine transport and presentation in HEV: a remote control mechanism for monocyte recruitment to lymph nodes in inflamed tissues. *J. Exp. Med*. 194:1361–1373. https://doi.org/10.1084/jem.194.9.1361

Perdiguero, E.G., and F. Geissmann. 2016. The development and maintenance of resident macrophages. *Nat. Immunol*. 17:2–8. https://doi.org/10.1038/ni.3341

Price, T.T., M.L. Burness, A. Sivan, M.J. Warner, R. Cheng, C.H. Lee, L. Olivere, K. Comatas, J. Magnani, H. Kim Lyerly, et al. 2016. Dormant breast cancer micrometastases reside in specific bone marrow niches that regulate their transit to and from bone. *Sci. Transl. Med*. 8. 340ra73. https://doi.org/10.1126/scitranslmed.aad4059

Prost, S., R.E. Kishen, D.C. Kluth, and C.O. Bellamy. 2016. Working with Commercially Available Quantum Dots for Immunofluorescence on Tissue Sections. *PLoS One*. 11. e0163856. https://doi.org/10.1371/journal.pone.0163856

Pyonteck, S.M., L. Akkari, A.J. Schuhmacher, R.L. Bowman, L. Sevenich, D.F. Quail, O.C. Olson, M.L. Quick, J.T. Huse, V. Teijeiro, et al. 2013. CSF-1R inhibition alters macrophage polarization and blocks glioma progression. *Nat. Med*. 19:1264–1272. https://doi.org/10.1038/nm.3337

Qian, B., Y. Deng, J.H. Im, R.J. Muschel, Y. Zou, J. Li, R.A. Lang, and J.W. Pollard. 2009. A distinct macrophage population mediates metastatic

breast cancer cell extravasation, establishment and growth. *PLoS One*. 4. e6562. https://doi.org/10.1371/journal.pone.0006562

Qian, B.Z., and J.W. Pollard. 2010. Macrophage diversity enhances tumor progression and metastasis. *Cell*. 141:39–51. https://doi.org/10.1016/j.cell.2010.03.014

Qian, B.Z., J. Li, H. Zhang, T. Kitamura, J. Zhang, L.R. Campion, E.A. Kaiser, L.A. Snyder, and J.W. Pollard. 2011. CCL2 recruits inflammatory monocytes to facilitate breast-tumour metastasis. *Nature*. 475:222–225. https://doi.org/10.1038/nature10138

Quail, D.F., and J.A. Joyce. 2017. Molecular Pathways: Deciphering Mechanisms of Resistance to Macrophage-Targeted Therapies. *Clin. Cancer Res*. 23:876–884. https://doi.org/10.1158/1078-0432.CCR-16-0133

Ritchie, M.E., B. Phipson, D. Wu, Y. Hu, C.W. Law, W. Shi, and G.K. Smyth. 2015. limma powers differential expression analyses for RNA-sequencing and microarray studies. *Nucleic Acids Res*. 43. e47. https://doi.org/10.1093/nar/gkv007

Ruffell, B., and L.M. Coussens. 2015. Macrophages and therapeutic resistance in cancer. *Cancer Cell*. 27:462–472. https://doi.org/10.1016/j.ccell.2015.02.015

Schulz, C., E. Gomez Perdiguero, L. Chorro, H. Szabo-Rogers, N. Cagnard, K. Kierdorf, M. Prinz, B. Wu, S.E. Jacobsen, J.W. Pollard, et al. 2012. A lineage of myeloid cells independent of Myb and hematopoietic stem cells. *Science*. 336:86–90. https://doi.org/10.1126/science.1219179

Sethi, N., X. Dai, C.G. Winter, and Y. Kang. 2011. Tumor-derived JAGGED1 promotes osteolytic bone metastasis of breast cancer by engaging notch signaling in bone cells. *Cancer Cell*. 19:192–205. https://doi.org/10.1016/j.ccr.2010.12.022

Shi, C., T. Jia, S. Mendez-Ferrer, T.M. Hohl, N.V. Serbina, L. Lipuma, I. Leiner, M.O. Li, P.S. Frenette, and E.G. Pamer. 2011. Bone marrow mesenchymal stem and progenitor cells induce monocyte emigration in response to circulating toll-like receptor ligands. *Immunity*. 34:590–601. https://doi.org/10.1016/j.immuni.2011.02.016

Shiozawa, Y., E.A. Pedersen, A.M. Havens, Y. Jung, A. Mishra, J. Joseph, J.K. Kim, L.R. Patel, C. Ying, A.M. Ziegler, et al. 2011. Human prostate cancer metastases target the hematopoietic stem cell niche to establish footholds in mouse bone marrow. *J. Clin. Invest*. 121:1298–1312. https://doi.org/10.1172/JCI43414

Sierra-Filardi, E., C. Nieto, A. Domínguez-Soto, R. Barroso, P. Sánchez-Mateos, A. Puig-Kroger, M. López-Bravo, J. Joven, C. Ardavín, J.L. Rodríguez-Fernández, et al. 2014. CCL2 shapes macrophage polarization by GM-CSF and M-CSF: identification of CCL2/CCR2-dependent gene expression profile. *J. Immunol*. 192:3858–3867. https://doi.org/10.4049/jimmunol.1302821

Stanley, E.R., K.L. Berg, D.B. Einstein, P.S. Lee, F.J. Pixley, Y. Wang, and Y.G. Yeung. 1997. Biology and action of colony--stimulating factor-1. *Mol. Reprod. Dev*. 46:4–10. https://doi.org/10.1002/(SICI)1098-2795(199701)46:1<4::AID-MRD2>3.0.CO;2-V

Van Rooijen, N., and A. Sanders. 1994. Liposome mediated depletion of macrophages: mechanism of action, preparation of liposomes and applications. *J. Immunol. Methods*. 174:83–93. https://doi.org/10.1016/0022-1759(94)90012-4

Varin, A., S. Mukhopadhyay, G. Herbein, and S. Gordon. 2010. Alternative activation of macrophages by IL-4 impairs phagocytosis of pathogens but potentiates microbial-induced signalling and cytokine secretion. *Blood*. 115:353–362. https://doi.org/10.1182/blood-2009-08-236711

Venmar, K.T., K.J. Carter, D.G. Hwang, E.A. Dozier, and B. Fingleton. 2014. IL4 receptor ILR4α regulates metastatic colonization by mammary tumors through multiple signaling pathways. *Cancer Res*. 74:4329–4340. https://doi.org/10.1158/0008-5472.CAN-14-0093

Wang, H., C. Yu, X. Gao, T. Welte, A.M. Muscarella, L. Tian, H. Zhao, Z. Zhao, S. Du, J. Tao, et al. 2015. The osteogenic niche promotes early-stage bone colonization of disseminated breast cancer cells. *Cancer Cell*. 27:193–210. https://doi.org/10.1016/j.ccell.2014.11.017

Weilbaecher, K.N., T.A. Guise, and L.K. McCauley. 2011. Cancer to bone: a fatal attraction. *Nat. Rev. Cancer*. 11:411–425. https://doi.org/10.1038/nrc3055

Wu, J.B., L. Yin, C. Shi, Q. Li, P. Duan, J.M. Huang, C. Liu, F. Wang, M. Lewis, Y. Wang, et al. 2017. MAOA-Dependent Activation of Shh-IL6-RANKL Signaling Network Promotes Prostate Cancer Metastasis by Engaging Tumor-Stromal Cell Interactions. *Cancer Cell*. 31:368–382. https://doi.org/10.1016/j.ccell.2017.02.003

Wynn, T.A., A. Chawla, and J.W. Pollard. 2013. Macrophage biology in development, homeostasis and disease. *Nature*. 496:445–455. https://doi.org/10.1038/nature12034

Xu, R., Y. Li, H. Yan, E. Zhang, X. Huang, Q. Chen, J. Chen, J. Qu, Y. Liu, J. He, et al. 2019. CCL2 promotes macrophages-associated chemoresistance via MCPIP1 dual catalytic activities in multiple myeloma. *Cell Death Dis*. 10:781. https://doi.org/10.1038/s41419-019-2012-4

Yanagihara, Y., K. Ikizawa, K. Kajiwara, T. Koshio, Y. Basaki, and K. Akiyama. 1995. Functional significance of IL-4 receptor on B cells in IL-4-induced human IgE production. *J. Allergy Clin. Immunol*. 96:1145–1151. https://doi.org/10.1016/S0091-6749(95)70199-0

Yang, M., D. McKay, J.W. Pollard, and C.E. Lewis. 2018. Diverse Functions of Macrophages in Different Tumor Microenvironments. *Cancer Res*. 78:5492–5503. https://doi.org/10.1158/0008-5472.CAN-18-1367

Zhang, X.H., Q. Wang, W. Gerald, C.A. Hudis, L. Norton, M. Smid, J.A. Foekens, and J. Massagué. 2009. Latent bone metastasis in breast cancer tied to Src-dependent survival signals. *Cancer Cell*. 16:67–78. https://doi.org/10.1016/j.ccr.2009.05.017

Zhu, Y., J.M. Herndon, D.K. Sojka, K.W. Kim, B.L. Knolhoff, C. Zuo, D.R. Cullinan, J. Luo, A.R. Bearden, K.J. Lavine, et al. 2017. Tissue-Resident Macrophages in Pancreatic Ductal Adenocarcinoma Originate from Embryonic Hematopoiesis and Promote Tumor Progression. *Immunity*. 47:323–338.e6. https://doi.org/10.1016/j.immuni.2017.07.014

Supplemental material

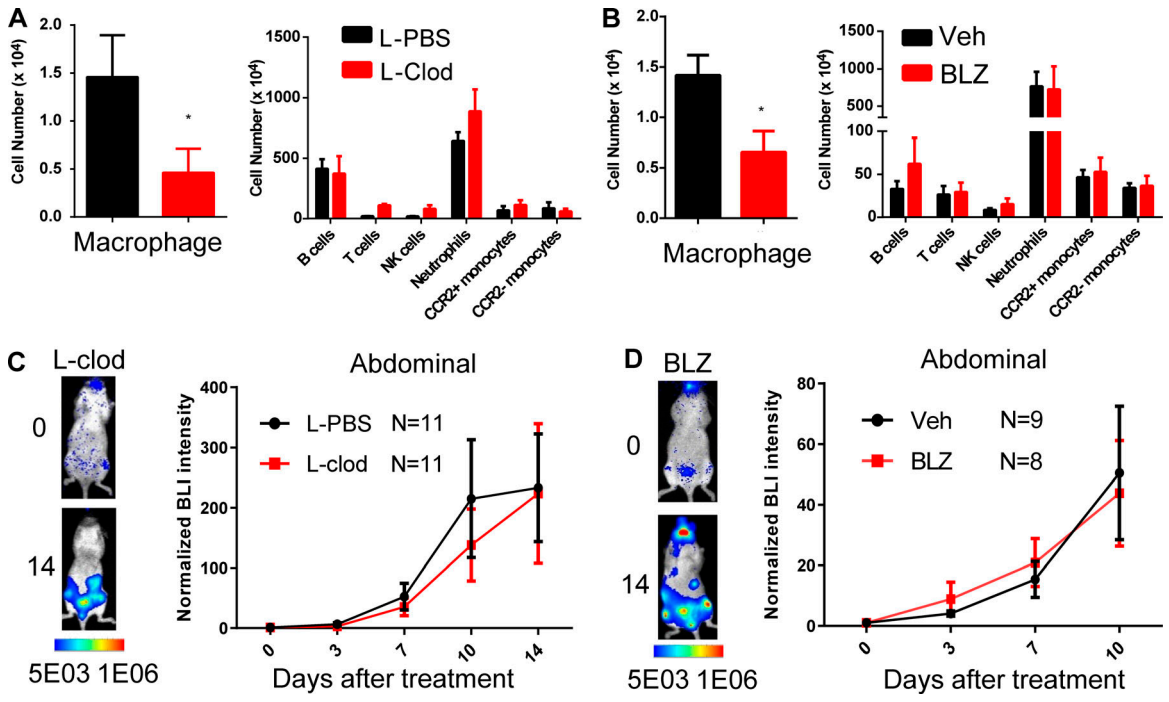

Figure S1. **Macrophage ablation does not affect other immune cells in bone or abdominal metastasis. (A)** FACS quantification of bone marrow immune cell populations from MetBo2 bone metastases treated with L-Clod, or control liposome (L-PBS). Bar represents SEM; *n* = 3 mice for each group. *, P < 0.05 with Student's *t* test. Experiments performed two times independently. NK, natural killer. **(B)** FACS quantification of bone marrow immune cell populations from MetBo2 bone metastases treated with CSF1R inhibitor, BLZ, and vehicle treatment. Bar represents SEM; *n* = 3 mice for each group. *, P < 0.05 with Student's *t* test. Experiments performed two times independently. **(C)** Quantification of bioluminescent signal of the abdominal lesion of MetBo2 cells in rare cases treated with L-Clod or corresponding vehicle (L-PBS). Signals were quantified by PhotonIMAGER and normalized to day 0. Bars represent SEM. N equals the number of mice included in quantification. Experiments performed three times independently. **(D)** Representative figures and quantification of bioluminescent signal of the abdominal lesion of MetBo2 cells in rare cases treated with BLZ945 (BLZ) or corresponding vehicle (Veh). Signals were quantified by PhotonIMAGER and normalized to day 0. Bars represent SEM. N equals the number of mice included in quantification. In mice with chest metastasis, only one mouse in vehicle group survived after 10 d. Experiments performed three times independently.

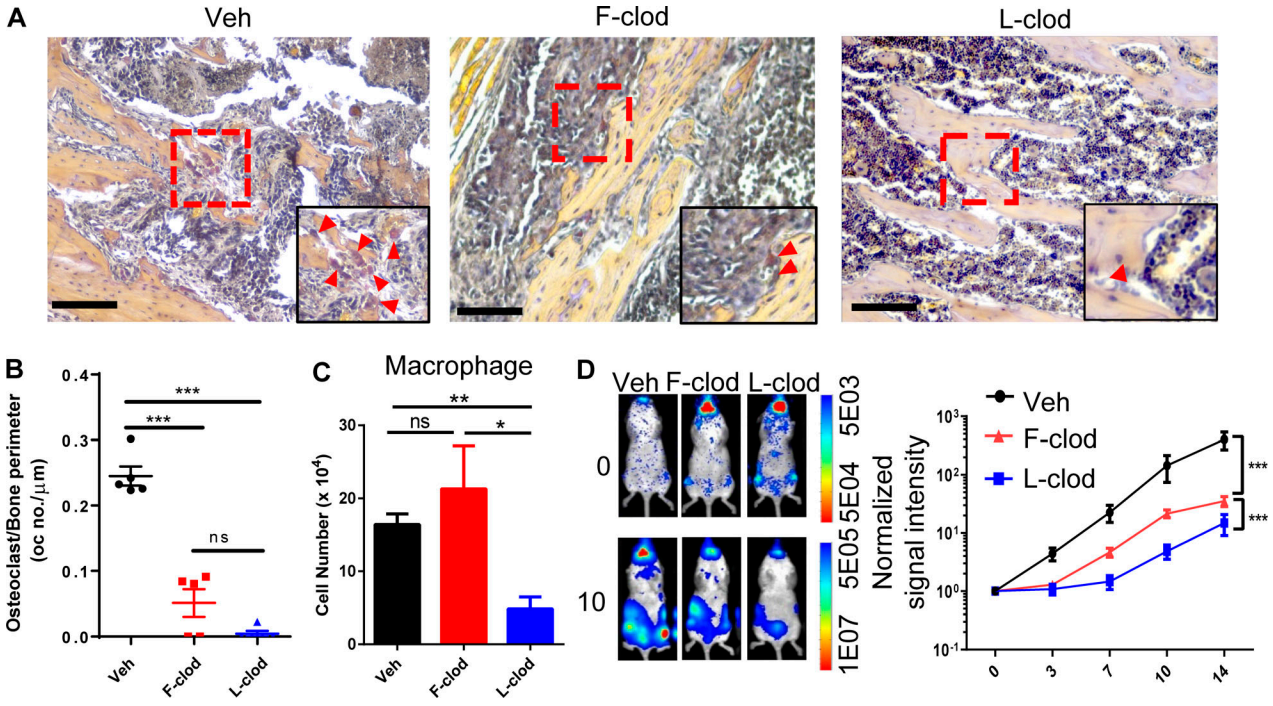

Figure S2. **Macrophages promote bone metastasis. (A)** Representative TRAP staining and quantification of MetBo2 bone metastasis. Sample treated with free clodronate (F-clod), L-Clod, or corresponding vehicles (Veh) until end point. Experiments performed two times independently. Bar = 20 µm. Red arrows indicate osteoclasts. **(B)** Quantification of osteoclasts in bone metastasis. ***, P < 0.001; ns, not significant. *n* = 5 for each group. **(C)** Quantification of macrophages in MetBo2 bone metastasis. Sample treated with free clodronate, L-Clod, or corresponding vehicles until the clinical end point. *n* = 3 for each group. *, P < 0.05; **, P < 0.01. Experiments performed two times independently. **(D)** Representative figures and quantification of bioluminescent signal of bone metastasis treated with free clodronate (F-clod), L-Clod, or corresponding vehicle (Veh) in MetBo2 murine breast cancer model. Signals were quantified by PhotonIMAGER and normalized to day 0. ***, P < 0.001. *n* = 6–8 mice for each group. Experiments performed two times independently.

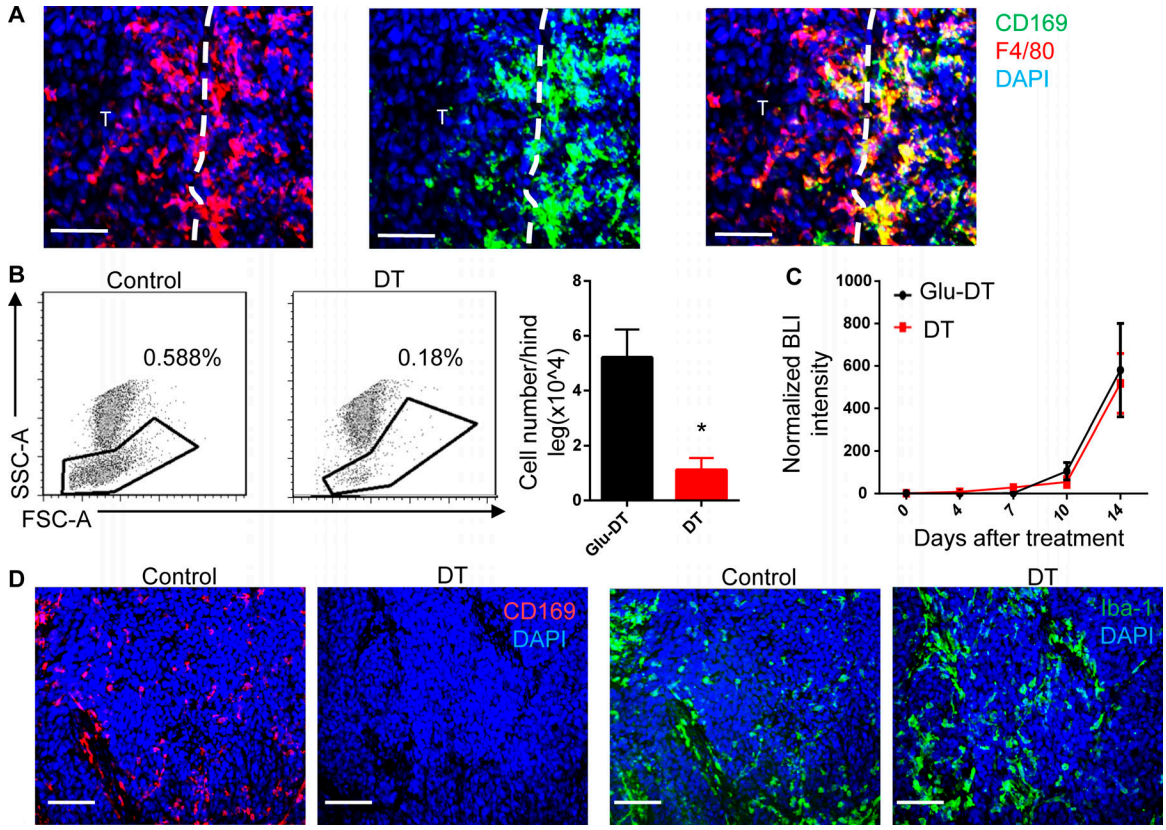

Figure S3. **CD169⁺ macrophages are dispensable for metastasis outgrowth. (A)** Representative immunofluorescent staining showing that most of the CD169⁺ macrophages do not infiltrate into bone metastasis. Bar = 50 µm. T, tumor area; green, CD169; red, F4/80; blue, DAPI. Experiments performed three times independently. **(B)** Representative FACS plot and quantification showing ablation of bone marrow macrophage ($CD11b^+F4/80^+SSC^{low}$, % of all immune cells) in mice treated with DT or control Glu-DT. Bars represent SEM; *n* = 3 mice for each group. *, P < 0.05 with Student's *t* test. **(C)** Quantification of bioluminescent (BLI) signal of MetBo2 bone metastasis in CD169-DTR mice treated with DT or Glu-DT. Signals were quantified by PhotonIMAGER and normalized to day 0. Bar represents SEM; *n* = 4–8 tumors for each group. **(D)** Representative immunofluorescent staining of MetBo2 bone metastasis in CD169-DTR mice showing depletion of CD169⁺ macrophages but not the majority of Iba1⁺ macrophages in DT-treated mice compared with control Glu-DT treatment. Bar = 50 µm. Red, CD169; blue, DAPI. In B–D, experiments were performed two times independently.

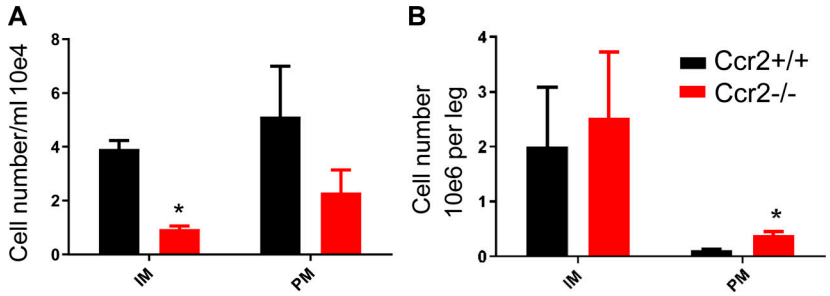

Figure S4. ***Ccr2*$^{-/-}$ mice are deficient in circulating but not bone marrow monocytes. (A)** Absolute number of IMs and PMs in blood of CCR2 knockout mice and WT mice. Bar represents SEM. *n* = 3 mice for each group. *, P < 0.05 with Student's *t* test. **(B)** Absolute number of IMs and PMs per leg in bone marrow of CCR2 knockout mice and WT mice. Bar represents SEM. *n* = 3 mice for each group. *, P < 0.05 with Student's *t* test. In A and B, experiments were performed three times independently.

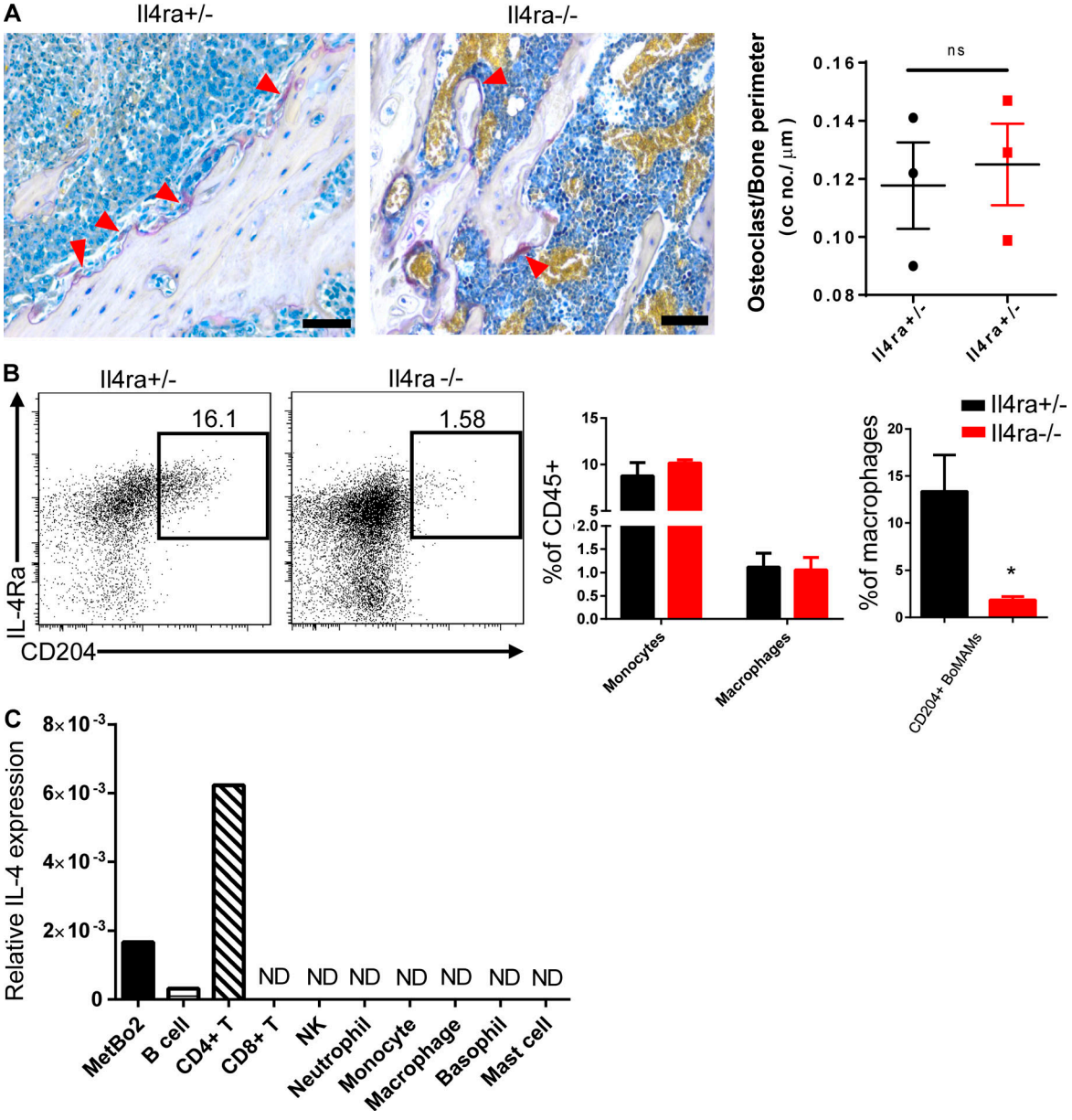

Figure S5. ***Il4ra*$^{-/-}$ affect BoMAM but not osteoclast. (A)** Representative TRAP staining (pink stain, red arrowheads) and quantification of 1833 bone metastasis from mosaic mice bearing *Il4r*$^{+/-}$ and *Il4r*$^{-/-}$ bone marrow. Bar = 20 µm; error bars represent SEM. *n* = 3 mice for each group. ns, not significant. **(B)** Representative FACS plot and quantification showing the change of monocytes, macrophages, and CD204^{+} BoMAMs in mosaic mice bearing *Il4r*$^{+/-}$ and *Il4r*$^{-/-}$ bone marrow. Bar represents SEM. *n* = 3 mice for each group. *, P < 0.05 with Student's *t* test. Experiments performed two times independently. **(C)** Representative image of relative expression of IL-4 in different cell types in MetBo2 bone metastasis. Immune cell populations and tumor cells from bone metastasis sample were sorted based on the lineage markers, and RNA was extracted for quantitative PCR. Each sample includes two mice, and the experiment was repeated two times. NK, natural killer.

Table S1 is provided online and shows clinical information for breast cancer bone patients.